Available online at www.sciencedirect.com
ScienceDirect
Advances in Space Research xxx (2007) xxx–xxx
ADVANCES IN SPACE RESEARCH (a COSPAR publication)
www.elsevier.com/locate/asr

A ballistic limit equation for hypervelocity impacts on composite honeycomb sandwich panel satellite structures

S. Ryan [a,b,*], F. Schaefer [a], R. Destefanis [c], M. Lambert [d]

[a] Fraunhofer-Institut für Kurzzeitdynamik, Ernst-Mach-Institut (EMI), Eckerstr. 4, D-79014 Freiburg, Germany
[b] School of Aerospace, Mechanical & Manufacturing Engineering, RMIT University, GPO Box 2476V, Melbourne, Australia
[c] Alcatel Alenia Space, Str. Antica di Collegno 253, 10146 Turin, Italy
[d] ESA-ESTEC, Postbus 299, NL-2200 AG Noordwijk, The Netherlands

Received 27 July 2006; received in revised form 7 February 2007; accepted 12 February 2007

Abstract

During a recent experimental test campaign performed in the framework of ESA Contract 16721, the ballistic performance of multiple satellite-representative Carbon Fibre Reinforced Plastic (CFRP)/Aluminium honeycomb sandwich panel structural configurations (GOCE, Radarsat-2, Herschel/Planck, BeppoSax) was investigated using the two-stage light-gas guns at EMI. The experimental results were used to develop and validate a new empirical ballistic limit equation (BLE), which was derived from an existing Whipple-shield BLE. This new BLE provided a good level of accuracy in predicting the ballistic performance of stand-alone sandwich panel structures. Additionally, the equation is capable of predicting the ballistic limit of a thin Al plate located at a standoff behind the sandwich panel structure. This thin plate is the representative of internal satellite systems, e.g. an Al electronic box cover, a wall of a metallic vessel, etc. Good agreement was achieved with both the experimental test campaign results and additional test data from the literature for the vast majority of set-ups investigated. For some experiments, the ballistic limit was conservatively predicted, a result attributed to shortcomings in correctly accounting for the presence of high surface density multi-layer insulation on the outer facesheet. Four existing BLEs commonly applied for application with stand-alone sandwich panels were reviewed using the new impact test data. It was found that a number of these common approaches provided non-conservative predictions for sandwich panels with CFRP facesheets.

Keywords: Space debris; Hypervelocity impact; Composites; CFRP; Damage laws; Ballistic limit equation

1. Introduction

Composite sandwich panels consisting of Carbon Fibre Reinforced Plastic facesheets bonded to Aluminium honeycomb cores (CFRP/Al HC SP) are amongst the most commonly used structures for satellites due to their relative low mass and high thermal and mechanical stability. However, the protective performance of these structure types with regards to hypervelocity space debris and micrometeoroid impacts is poor compared to that of more traditional structural wall types (e.g. an Al Whipple shield). With the growing number of debris particles in Earth orbit, the need to characterise the risk of these particles on the successful fulfilment of mission objectives becomes increasingly critical.

To assess the threat of micrometeoroid/orbital debris (M/OD) on a satellite mission, equations that define the limits of structural perforation in terms of impactor mass, velocity and angle are required. This type of equation is referred to as a ballistic limit equation (BLE). For risk assessment of satellite structures ballistic equations derived for application with metallic Whipple shields are commonly applied. However, it is recognised that, unlike for manned spacecraft, a perforation event is not necessarily

* Corresponding author. Address: Fraunhofer-Institut für Kurzzeitdynamik, Ernst-Mach-Institut (EMI), Eckerstr. 4, D-79014 Freiburg, Germany. Tel.: +49 7612714402; fax: +49 7612714316.
E-mail addresses: shannon.ryan@emi.fhg.de (S. Ryan), frank.schaefer@emi.fhg.de (F. Schaefer).

0273-1177/$30 © 2007 Published by Elsevier Ltd on behalf of COSPAR.
doi:10.1016/j.asr.2007.02.032

Nomenclature

Notation & Acronyms

AD	areal density (g/cm^2)
AXAF	Ad. X-ray astrophysics facility CFRP/Al HC SP
BLC	ballistic limit curve
BLE	ballistic limit equation
CFRP	Carbon Fibre Reinforced Plastic
DSP	impact test result – detached spall
ENV	Envisat CFRP/Al HC SP
GOCE	GOCE CFRP/Al HC SP (central cylinder panel)
HC	honeycomb
HVI	hypervelocity impact
H/P	Herschel/Planck CFRP/Al HC SP (closure panel)
MLI	multi-layer insulation
M/OD	micrometeoroid/orbital debris
NSP	impact test result – no detached spall
P	impact test result – perforation
RAD1	Radarsat-2 CFRP/Al HC SP (+/−Z panel)
RAD2	Radarsat-2 CFRP/Al HC SP (shear panel)
RAD3	Radarsat-2 CFRP/Al HC SP (cone panel)
SAX	BeppoSax CFRP/Al HC SP (optical bench)
SP	sandwich panel
WP	witness plate
c_B	bulk sound speed
d_c^{SP}	critical projectile diameter for SP structure (cm)
d_c^{SP+WP}	critical projectile diameter for SP+WP structure (cm)
K	slope of shock velocity–particle velocity diagram
S_1	spacing between outer bumper and bumper plate (cm)
S_2	spacing between bumper and rear wall (cm)
t	thickness
v	impact velocity (km/s)
ρ	material density (g/cm^2)
q	impact angle (°)
σ_y	yield strength (ksi)

Subscripts:

b	bumper (SP rear facesheet/Whipple-shield rear wall)
ob	outer bumper (SP front facesheet/Whipple-shield bumper)
p	projectile
w	backwall
MET	modified ESA triple wall equation
SRL	Schaefer Ryan Lambert BLE

critical for satellite structures. It is only when internal systems essential to the satellite function become inoperable that the impact event is, by definition, critical. Thus, for more accurate risk assessment of satellite structures, equations that allow for these more specific failure mechanisms to be predicted are required. Currently, no validated BLEs existing for application in the risk assessment of CFRP/Al HC satellite structures are available.

2. Hypervelocity impact tests on CFRP/Al HC SP structures

2.1. Overview of the test program

In the framework of ESA Contract 16721/02/NL/CK (Schaefer and Ryan, 2005) an extensive experimental campaign was performed to investigate the ballistic limit of various CFRP/Al HC SP structures and thin Al plates located behind the structure walls at a standoff. A total of 55 impact tests were performed at a range of impact velocities and angles on six representative satellite structures. Given that perforation does not necessarily represent critical failure for a satellite mission, 15 of the experiments were performed at impact conditions substantially above the respective SP ballistic limit in order to define the penetration conditions of the thin Al plate located at a standoff of 100 mm behind the SP rear facesheet. Some preliminary results of this test campaign were presented in Schaefer et al. (2005).

2.2. Test samples

Given that CFRP/Al HC SP structures are very often configured for specific requirements, any predictive BLE must be general enough to be applied across a large range of configurations with very different properties, including constituent mechanical properties, facesheet layups, facesheet thickness and honeycomb depth, honeycomb properties (cell size and wall thicknesses), etc. As such, panels tested in the experimental campaign were selected for both their relevance to satellite application and to provide a wide range of different configurations.

Three different sandwich panels were tested from the Radarsat-2 satellite (the +/−Z, shear, and cone panels RAD1, RAD2, and RAD3, respectively), in addition to the GOCE central cylinder panel (GOCE), BeppoSax optical bench (SAX), and Herschel/Planck closure panels (H/P). Details of the various panels are described in Table 1.

The distribution of panel characteristics is shown in Fig. 1.

2.3. Test set-up

All impact tests were performed on EMI's two-stage light-gas guns. An overview of the operating principles of two-stage light-gas guns is given in Schneider and Schaefer (2001). All impact experiments used spherical Al projectiles (2017-T4 for projectiles 1.25 mm or smaller, 99.98% pure

Table 1
An overview of the panels impacted during the experimental campaign

Panel	AD (g/cm^2)	Facesheets			Honeycomb	
		t (mm)	Material	Stacking	Configuration	t (mm)
RAD1	0.7017	1.45	FL01 (F)-HMF196/34 T300-1k fabric FL02 (P)-HYE 4934C K139 u.d. ply	$(0_F/0_P/+45_P/90_P/-45_P/-45_P/90_P/+45_P/0_P)$	3/16-5056-.001P	50.6
RAD2	0.5847	1.40	FL01(F)-HMF196/34 T300-1k fabric FL02(P)-HYE 4934C K139 u.d. ply	$(+45_F/0_P/-45_P/+45_P/90_P)_S$	3/16-5056-.001P	25.3
RAD3	0.4217	1.15	FL01(F)-HMF196/34 T300-1k fabric FL02(P)-HYE 4934C K139 u.d. ply	$(0_F/0_F/+9_P/-9_P/+9_P/-9_P/+9_P/-9_P/0_F/0_F)$	3/16-5056-.001P	12.1
GOCE	0.7807	2.30	M18/32%/M55J/145 u.d. ply	$(+45/0_2/-45/0_2/+45/0_2/-45/0_2/+45/0_2/-45)$	3/16-5056-.001P	12.5
SAX	0.4405	0.95	914/34%/137/6K/M40B u.d. ply	$(0/+60/-60)_S$	3/16-5056-.001P	29.7
H/P	0.2300	0.55	M18/G801 u.d. ply	$(+45/0/90/-45)$	3/16-5056-.0007P	19.9

aluminium for others) which are housed in a plastic cylinder (sabot) during the acceleration process. After exiting the launch tube, the sabot parts are separated from the projectile by aerodynamic drag and the projectile passes through dual laser light barriers which record the velocity before impacting the target. Impact tests were performed in medium vacuum (200 mbar $\leqslant P \leqslant$ 6E−02 mbar). To account for the different target chamber residual pressures, the velocity measurements were adjusted for drag effects.

In all tests an Al plate was spaced at 100 mm, measured from the panel rear. In the sandwich panel ballistic limit experiments, these plates were 0.5 mm thick Al 2024 T3. For tests assessing the ballistic limit of a thin Al plate located behind the structure wall, the plates were 1.5 mm thick Al 7075. The material, thickness and offset of this plate was selected based on results of a literature review to best represent the lid of an electronic box structure.

2.4. Definition of failure

The test results were defined as "perforated" (P), "detached spall" (DSP), or "no detached spall" (NSP). A perforated sample showed a clear, measurable hole in the sandwich panel rear facesheet or witness plate as shown in Fig. 3a. Detached spall refers to the case in which material was spalled from the rear facesheet of the sandwich panel or rear side of the witness plate when no clear perforation hole exists. An example of a detached spall result is shown in Fig. 3b. No detached spall represents no visible damage on the target rear side.

2.5. Test results

The impact conditions and results of the 55 ballistic limit tests are provided in Table 3 (SP + WP impact tests) and Table 4 (stand-alone SP impact tests). Damage measurements made on the samples (both sandwich panel and witness plate) are defined in Table 2 and shown in Fig. 2.

3. A ballistic limit equation for application with CFRP/Al HC satellite structures

3.1. State-of-the-art

Schaefer et al. (2004) identified four different approaches for predicting the ballistic limit of CFRP/Al HC sandwich panel structures, all of which are based on the Christiansen/modified Cour-Palais Whipple-shield equation (Christiansen, 1993). The Whipple-shield equation is reproduced from Christiansen (1993) here. It should be noted that the nomenclature has been modified from the original publication.

Ballistic regime ($v_n \leqslant$ 3 km/s):

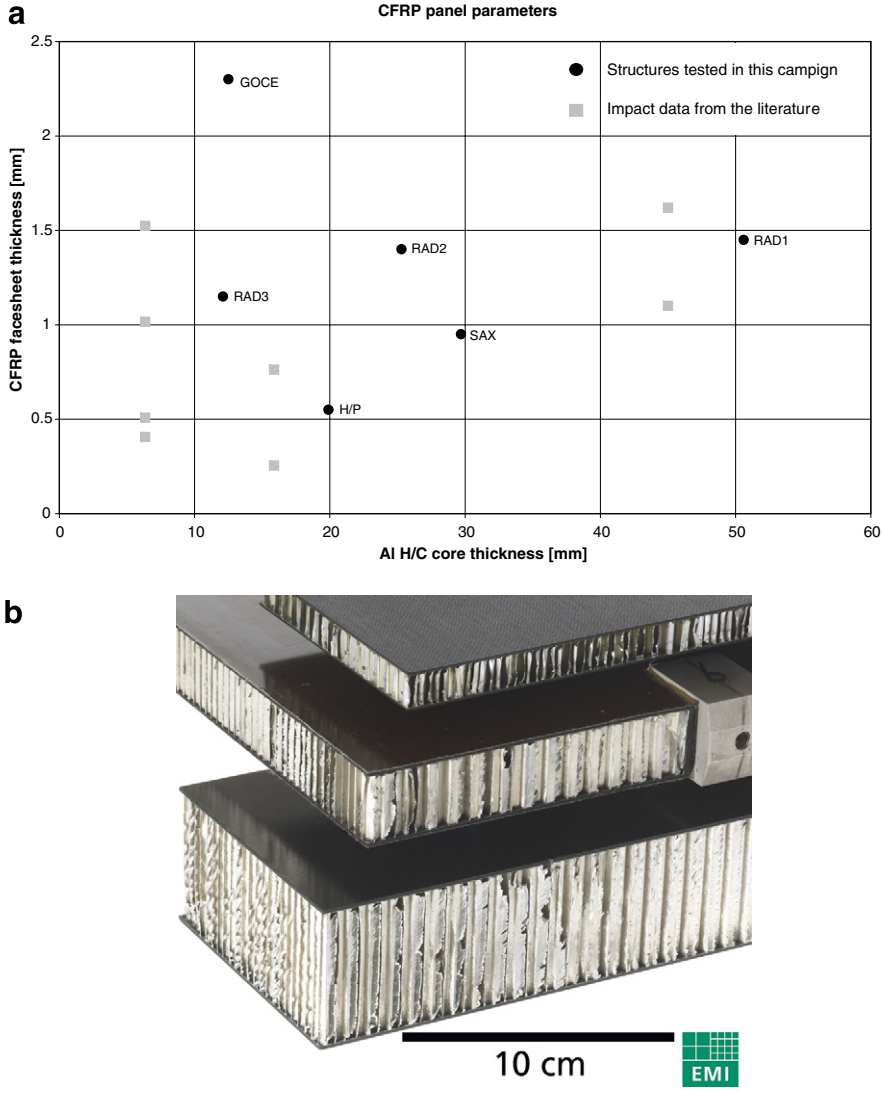

Fig. 1. (a) Distribution of CFRP facesheet and Al HC core thicknesses of the test samples and structures for which existing impact data is available; (b) photo of the three different Radarsat-2 panels used in impact experiments.

$$d_c = \left[\frac{t_b \cdot (\sigma/40)^{0.5} + t_{ob}}{0.6 \cdot (\cos\theta)^{5/3} \cdot \rho_p^{0.5} \cdot v^{2/3}}\right]^{18/19} \quad (1)$$

Transition/shatter regime ($3 < v_n < 7$ km/s):

$$d_c = \left[\frac{t_b \cdot (\sigma/40)^{0.5} + t_{ob}}{1.248 \cdot \rho_p^{0.5} \cdot \cos\theta}\right]^{18/19} \times \left[1.75 - \frac{(v \cdot \cos\theta)}{4}\right] \cdots + \left[\frac{1.071 \cdot t_b^{2/3} \cdot S^{1/3}(\sigma/70)^{1/3}}{\rho_p^{1/3} \cdots \rho_{ob}^{1/9}}\right] \times \left[\frac{(v \cdot \cos\theta)}{4} - 0.75\right] \quad (2)$$

Hypervelocity regime ($v_n \geqslant 7$ km/s):

$$d_c = \left[\frac{3.918 \cdot t_b^{2/3} \cdot S^{1/3}(\sigma/70)^{1/3}}{\rho_p^{1/3} \cdot (v \cdot \cos\theta)^{2/3} \cdot \rho_{ob}^{1/9}}\right] \quad (3)$$

The four different approaches are referred to herein as:

1. Taylor (Taylor et al., 1999);
2. Frost approach 1 (Frost and Rodriguez, 1997);
3. Frost approach 2 (Frost and Rodriguez, 1997);
4. Modified ESA Triple Wall, MET (Schaefer et al., 2004).

The Taylor equation applies the Christiansen/Cour-Palais equation (Eqs. (1)–(3)) by calculating the thickness of Aluminium plates with the equivalent areal density of the CFRP facesheets. The Al-equivalent rear wall is then multiplied by a scaling factor, recommended as 0.5, based on experimental data. The honeycomb core depth is used as the Whipple-shield spacing; S. Parameters of the Whipple-shield equation modified in the Taylor approach are defined in Table 4.

Frost and Rodriguez present two approaches to calculate the ballistic limit of the CFRP/Al HC sandwich panel from the AXAF satellite. In Frost approach 1, Eqs. (1)–(3) are used with the composite material properties and thick-

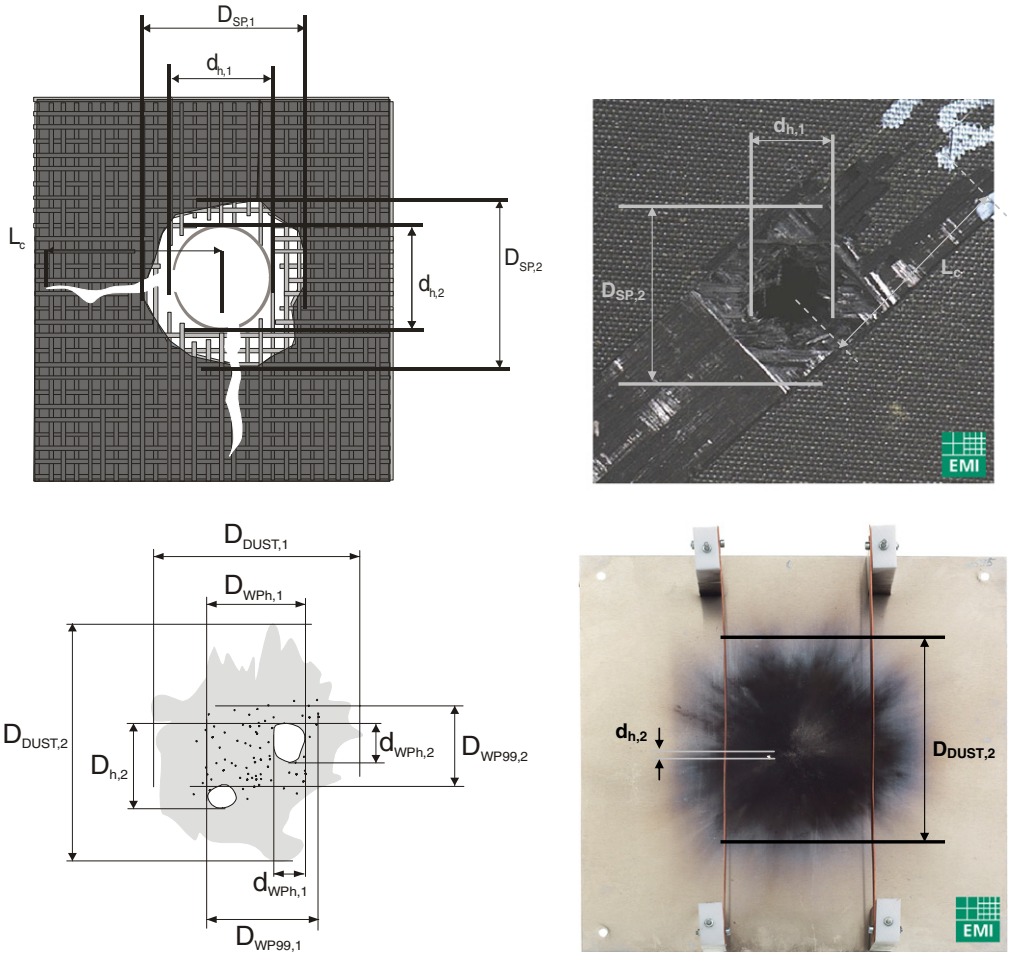

Fig. 2. Damage measurements. Upper: sandwich panel facesheets; lower: witness plate.

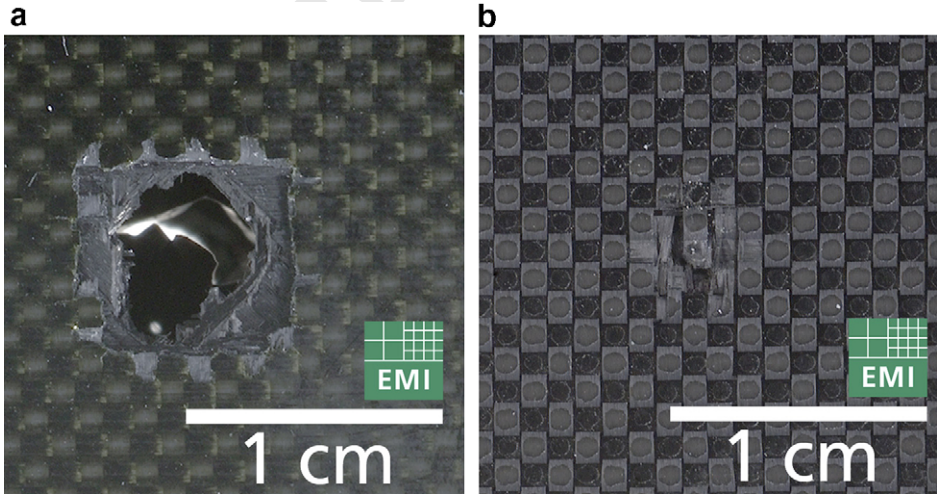

Fig. 3. Photos showing (a) "perforated" and (b) "detached spall" result.

nesses as if they were aluminium (as shown in Table 5). Frost approach 2 calculates equivalent Al-plate thicknesses, similar to the Taylor approach, but the thicknesses are calculated using both the density and yield strength of the CFRP and reference Al materials (see Table 5). The Frost approaches are the only ones which consider the actual properties of the CFRP material beyond its density.

The MET approach presented by Schaefer is based on the ESA Triple Wall equation (Drolshagen and Borge, 1992). The approach includes two coefficients (K_{3S} and K_{3D}) which are adjustable for use on structures different

Table 2
Damage measurement notation and indices

Notation	
Front and rear facesheets	
d_h	Clear hole diameter
D_{SP}	Diameter of surface spall area
L_C	Length of crack extension in fibre direction (impact centre to tip of crack)
Witness plate	
d_{WPh}	Maximum perforation hole diameter
D_{WPh}	Diameter of area containing perforation holes
D_{DUST}	Diameter of area covered with dust
D_{WP99}	Maximum diameter covering 99% of cratered area
Indices	
1	Horizontal
2	Vertical
ave	Average

to a metallic Whipple shield. It should be noted that the ESA Triple Wall equation is exactly the same as Eqs. (1)–(3) for the case $K_{3S} = 1$ and $K_{3D} = 0.16$. In contrast to the Christiansen/Cour-Palais equation, however, the ESA Triple Wall equation does not define a limit angle (angle where the projectile critical diameter does not further increase with increasing impact angle). The MET approach uses the same density-based method as the Taylor approach to calculate the thickness of equivalent Aluminium plates for the CFRP facesheets. Additionally, a multiplier g_i is included to enable definition between different failure types (detached spallation and clear hole perforation). The modified parameters of the Whipple-shield equation are given in Table 5.

3.2. The SRL ballistic limit equation

The new equation, referred to herein as the Schaefer Ryan Lambert (SRL) equation, is based on the ESA Triple Wall equation (ETW) from (Drolshagen and Borge (1992)). As mentioned previously, the ETW equation does not define a limit angle (angle at which increasing impact obliquity does not further affect the critical projectile diameter), which is set as 65° in the Christiansen/Cour-Palais equation. The assumption that at angles above 65° the primary source of rear wall damage are fragments of the front facesheet has been adopted here, thus the 65° limit angle of Christiansen/Cour-Palais was adopted.

The equation is used to predict the critical projectile diameter (d_c) which, at a given impact velocity and angle, will perforate the structure under consideration. The BLE can be applied to calculated the critical projectile diameter for both stand-alone CFRP/Al HC sandwich panels (d_c^{SP}) and CFRP/Al HC SP structures with a thin Al plate placed behind it at a standoff (d_c^{SP+WP}). The principle set-up is shown in Fig. 4.

The SRL BLE is given below:

Ballistic regime ($v_n \leqslant 4.2$ km/s):

$$d_c(v) = \left[\frac{\frac{\left(t_w^{1/2} + t_b\right)}{K_{3S}} \cdot \left(\frac{\sigma_y}{40}\right)^{1/2} + t_{ob}}{0.6 \cdot (\cos\theta)^{4/3} \cdot \rho_p^{1/2} \cdot v^{2/3}} \right]^{18/19} \quad (4)$$

Transition/shatter regime ($4.2 < v_n < 8.4$ km/s):

$$d_c(v) = d_c(v_1) + \frac{d_c(v_2) - d_c(v_1)}{v_2 - v_1} \cdot (v - v_1)$$
$$v_1 = \frac{4.2 \text{ km/s}}{\cos\theta} \quad (5)$$
$$v_2 = \frac{8.4 \text{ km/s}}{\cos\theta}$$

Hypervelocity regime ($v_n \geqslant 8.4$ km/s):

$$d_c(v) = \frac{1.155 \cdot \left(S_1^{1/3} \cdot (t_b + t_w)^{2/3} + S_2^{1/3} \cdot t_w^{2/3}\right) \cdot \left(\frac{\sigma_y}{70}\right)^{1/3}}{K_{3D}^{2/3} \cdot \rho_p^{1/3} \cdot \rho_b^{1/9} \cdot v^{2/3} \cdot \cos\theta^{4/3}} \quad (6)$$

Table 3
Ballistic limit test results of CFRP/Al HC sandwich panels with witness plate

Panel	EMI No.	v (km/s)	α (°)	d_p (mm)	m_p (mg)	E_k (J)	Result		WP damage (mm)			
							SP	WP	d_{WPh}	D_{WPh}	D_{DUST}	D_{WP99}
RAD1	S-4671	2.6	0	4.0	87.5	296	*P*	*P*	2.9	2.7 × 3.1	50 × 54	33 × 13
	S-4672	3.57	0	4.0	87.1	555	*P*	*P*	1.6	16.8 × 9.1	100 × 84	106 × 70
	S-4673	6.47	0	4.0	86.5	1810	*P*	*P*	1.75	5.8 × 4.8	150 × 190	28 × 27
	S-4616	6.99	0	4.0	87.2	2131	*P*	*P*	1.4	1.4 × 1.4	145 × 145	42 × 40
	S-4682	7.75	0	4.0	86.9	2610	*P*	NSP	No hole		150 × 155	16 × 13
	S-4617	6.91	45	4.0	87.5	2089	*P*	NSP	No hole		95 × 77	–
	S-4618	6.85	45	5.0	176	4129	*P*	NSP	No hole		105 × 185	–
	S-4695	6.45	0	4.0	87.7	1824	*P*	*P*	2.2	1.8 × 2.6	150 × 130	56 × 54
	S-4694	6.53	0	4.0	86.8	1851	*P*	*P*	15.0	15.6 × 14.5	90 × 98	51 × 56
RAD3	S-4610	6.73	0	3.0	37.1	840	*P*	DSP	No hole		165 × 150	70 × 70
	S-4611	6.72	0	4.0	87.5	1976	*P*	*P*	2.5	10 × 17	230 × 235	81 × 99
GOCE	S-4693	4.13	0	4.0	87.3	745	*P*	NSP	No hole		47 × 51	62 × 78
	S-4692	6.40	0	4.0	87.4	1790	*P*	DSP	No hole		140 × 117	72 × 50
SAX	S-4621	6.92	0	4.0	87.4	2093	*P*	*P*	3.35	11.0 × 11.4	205 × 190	85 × 80
	S-4622	6.64	45	4.0	86.7	1911	*P*	NSP	No hole		160 × 190	–

Please cite this article in press as: Ryan, S. et al., A ballistic limit equation for hypervelocity impacts ..., J. Adv. Space Res. (2007), doi:10.1016/j.asr.2007.02.032

Table 4
Ballistic limit test results of CFRP/Al HC sandwich panels

Panel	EMI No.	v (km/s)	α (°)	d_p (mm)	m_p (mg)	E_k (J)	Coarse result	Front FS (mm)		Rear FS (mm)	
								$d_{h,ave}$	d_{sp}	$d_{h,ave}$	d_{sp}
RAD1	B-107	2.02	0	1.25	2.9	2.9	NSP	2.3	5.0×4.7	No damage	
	B-106	2.36	0	1.0	1.3	1.8	DSP	2.2	4.2×5.8	–	1.5×0.7
	B-164	3.13	0	1.5	5.61	27	*P*	4.29	7.9×4.7	3.6	7.4×6.5
	B-119	6.24	0	1.0	1.2	20	*P*	4.3	8.3×8.9	3.1	5.9×7.7
	B-117	6.27	0	1.0	1.2	24	*P*	4.5	8.6×7.6	1.1	5.6×4.2
	S-4577	5.72	0	1.5	5.4	88	*P*	5.74	8.5×10	6.42	9.9×11.3
	S-4578	5.72	0	1.5	5.4	88	*P*	6.07	7.2×9.8	5.96	11.1×11.7
	B-108	6.27	0	1.5	5.6	110	*P*	6.19	9.4×9.8	6.16	8.5×9.6
	B-161	4.27	45	1.0	1.52	14	NSP	3.2	6.5×6.2	No damage	
	B-167	3.39	45	1.25	2.87	17	NSP	3.5	6.4×8.3	No damage	
	S-4579	5.87	45	1.5	5.3	91	NSP	5.96	8.3×10.0	No damage	
	S-4580	6.12	45	2.0	11.8	221	DSP	7.7	10.6×10.1	–	4.0×3.2
	S-4583	6.07	60	2.0	12	221	*P*	7.6	10.2×11.7	0.9	3.7×4.3
	S-4582	6.52	60	2.5	21	446	*P*	9.3	12.1×13.2	6.6	11.7×15.2
	S-4581	6.23	60	3.0	37.2	722	*P*	10.3	11.2×14.4	6.4	8.7×9.3
RAD 2	B-149	5.93	0	1.0	1.6	28	NSP	4.4	8.2×7.8	No damage	
	B-155	6.26	0	1.25	2.88	56	*P*	5.1	8.7×8.7	5.9	13.6×14.4
	S-4612	6.62	0	2.0	11.9	262	*P*	7.2	9.2×10.2	7.1	8.5×7.5
	B-150	5.96	45	1.0	1.56	28	NSP	4.5	7.0×8.1	No damage	
	S-4613	5.48	45	1.5	5.09	97	*P*	6.4	8.7×8	1.0	3×5
RAD3	B-105	2.82	0	1.0	1.3	2.5	*P*	2.3	3.0×3.0[a]	1.5	4.3×3.5
	B-139	3.36	0	1.0	1.51	8.5	*P*	2.3	3.7×2.5	1.0	1.9×4.1
	B-127	5.88	0	0.50	0.4	6.9	NSP	1.5	3.3×2.0	No damage	
	B-131	5.88	0	0.50	0.4	6.9	NSP	1.4	2.5×2.6[b]	No damage	
	B-132	6.05	0	0.70	0.45	8.2	NSP	2.2	4.2×4.1	No damage	
	B-154	5.94	0	0.80	0.31	16	DSP	2.6	4.4×2.9	–	0.5×0.5
	B-147	5.87	0	1.0	1.68	29	*P*	3.4	5.6×4.8	4.7	8.2×9.6
	B-162	3.42	45	1.0	1.51	8.8	NSP	2.6	3.4×4.2	No damage	
	B-140	3.33	45	1.25	2.92	16	DSP	3.4	5.2×4.7	–	2.2×1.8
	B-156	6.45	45	0.80	1.46	30	NSP	3.6	4.3×5.7	No damage	
	B-133	6.18	45	1.0	1.44	28	DSP	3.6	4.7×4.5	<0.5	3.5×2.7
	B-160	6.62	60	1.0	2.05	45	NSP	3.8	4.5×5.8	No damage	
	B-134	5.77	60	1.55	5.48	91	*P*	5.7	6.5×8.4	5.3	10.1×4.4
	B-138	2.96	0	0.0761	0.55	2.4	NP	Not measured		No damage	
GOCE	B-146	5.98	0	1.0	1.57	28	NSP	3.7	30.1×39.0	No damage	
	B-152	6.26	0	1.5	5.85	115	*P*	6.5	29.0×28.7	5.5	57.9×61.8
	B-145	5.80	45	1.0	1.52	26	NSP	3.7	9.8×9.9	No damage	
SAX	B-153	5.94	0	0.80	0.91	16	NSP	3.1	3.6×8.3	No damage	
	B-148	5.96	0	1.0	1.52	27	*P*	3.4	4.4×8.8	4.3	13.6×46.5
H/P	B-176	5.93	0	1.0	1.73	30	*P*	2.6	3.2×4.0	5.5	6.1×8.8

[a] Overlap from sabot part impact damage.
[b] Overlap of spall area from two tests. Average measurement taken.

Table 5
The variation of Whipple-shield equation parameters for application with CFRP/Al HC SPs

Parameter	Frost and Rodriguez (approach1)	Frost and Rodriguez (approach 2)	Taylor	Schaefer
t_{ob}	$t_{ob,CFRP}$	$t_{ob,CFRP} \cdot \left(\frac{\rho_{Al}}{\rho_{CFRP}}\right)^{-0.159} \cdot \left(\frac{\sigma_{Al}}{\sigma_{CFRP}}\right)^{-0.236}$	$t_{ob,CFRP} \times \frac{\rho_{CFRP}}{\rho_{Al}}$	$t_{ob,CFRP} \times \frac{\rho_{CFRP}}{\rho_{Al}}$
t_b	$t_{b,CFRP}$	$t_{b,CFRP} \cdot \left(\frac{\rho_{Al}}{\rho_{CFRP}}\right)^{-0.159} \cdot \left(\frac{\sigma_{Al}}{\sigma_{CFRP}}\right)^{-0.236}$	$0.5 \times t_{ob}$	$t_{b,CFRP} \times \frac{\rho_{CFRP}}{\rho_{Al}}$
σ_y	$\sigma_{y,CFRP}$	$\sigma_{y,Al}$	$\sigma_{y,Al}$	$\sigma_{y,Al}$
ρ_{ob}	ρ_{CFRP}	ρ_{Al}	ρ_{Al}	ρ_{Al}
S	t_{HC}	t_{HC}	t_{HC}	t_{HC}

An overview of the constants and parameters for use with the equation is given in Table 6.

The assumptions made in the new equation are:

(1) The space-facing (front) facesheet of the sandwich panel, having a thickness of t_{ob} (index ob = "outer bumper") is replaced by an Aluminium plate having

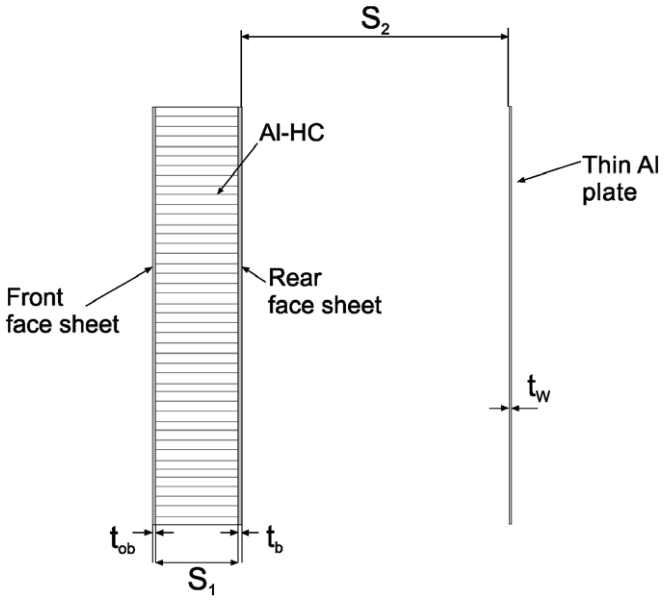

Fig. 4. Principle set-up for application of the SRL BLE.

Table 6
Ballistic limit equation parameter list for application with CFRP/Al HC SP structures

Parameter	Description	Suggested value
ρ	Density of reference Al-alloy (Al 2024 T81)	2.78 g/cm^3
σ_y	Yield strength of reference alloy (Al 2024 T81)	59.5 ksi
t_{ob}	Front facesheet thickness	$t_{ob,CFRP} \cdot \frac{\rho_{CFRP}}{2.78} + \frac{AD_{MLI}}{2.78}$
t_b	Rear facesheet thickness	$t_{b,CFRP} \cdot \frac{\rho_{CFRP}}{2.78}$
t_w	Al-plate thickness	
S_1	Spacing between facesheets	t_{HC}
S_2	Spacing between SP rear facesheet and Al-plate	
K_{3S}	Ballistic fit factor	1.1
K_{3D}	Hypervelocity fit factor	0.4

the same areal weight as the CFRP facesheet. The same procedure is repeated for the inner facesheet, having a thickness of t_b (index b = "bumper").

(2) The effects on fragmentation and expansion of the projectile fragment cloud caused by the presence of the sandwich panel honeycomb core, having a thickness S_1, were ignored. The presence of the honeycomb core acts to restrict expansion of the debris cloud following penetration of the front facesheet, concentrating or channelling the debris within a finite number of honeycomb cells. The effect of channelling on the protective capability of debris shielding remains somewhat conflicted. For instance, Jex et al. (1970) found that in velocity regimes inducing solid fragmentation of the projectile, the honeycomb core increases the ballistic protective capability compared to a standard Whipple-shield structure as secondary impacts of fragments on honeycomb cell walls lead to further fragmentation, overshadowing the detrimental effect of fragment channelling. Alternatively, Taylor (1999) introduced a ballistic limit equation for metallic sandwich panels which realized the channelling effect by decreasing the effective thickness of a Whipple-shield rear wall by a factor of two (across all impact angles and velocities).The honeycomb cores of the structures tested in this study all have, with the exception of the H/P closure panel, the same honeycomb core configuration (3/16″ cell size, 0.001″ foil thickness, Al5056 alloy). As such, the experimental data is insufficient to enable the effects of the honeycomb core properties, beyond core depth, to be characterised. Thus, the effect of the honeycomb core on the protection capability is taken into account by fit coefficients and a $\cos\theta$ dependence of the BLE.

(3) The ballistic effect of MLI placed on top of the space-facing facesheet of the sandwich panel can be accounted for by increasing the effective Aluminium facesheet thickness by an amount equal to the surface weight of the MLI. It should be noted that there were no impact tests performed on configurations with MLI in this study, hence the validity of this treatment method must still be proven in future test campaigns.

(4) The Aluminium plate located behind the CFRP H/C SP structure wall at a standoff of S_2 has a thickness of t_w (index w = "backwall"). In the ballistic velocity regime, S_2 does not need to be considered because it is assumed that the projectile does not fragment upon impact on the CFRP H/C SP. This assumption is in line with that applied by Christiansen (1993) for the BLE of metallic Whipple shields.

(5) Given that the equation is applied to calculate the ballistic limit of two different structure types (CFRP H/C SP and CFRP H/C SP + witness plate), an important requirement for the equation is that of convergence. When either the thickness or standoff of the witness plate approaches zero, the predicted ballistic limit converges to the stand-alone CFRP H/C SP result, i.e.:

$$d_c^{(SP+WP)}(v, t_{ob}, t_b, t_w, S_1, S_2) \xrightarrow{t_w \to 0} d_c^{(SP)}(v, t_{ob}, t_b, S_1)$$

and (7)

$$d_c^{(SP+WP)}(v, t_{ob}, t_b, t_w, S_1, S_2) \xrightarrow{S_2 \to 0} d_c^{(SP)}(v, t_{ob}, t_b + t_w, S_1)$$

6: Fitting of the equation to the experimental results is performed by modification of the following terms:

Fit parameter	Description
K_{3S}	ESA TW fit factor (ballistic regime)
K_{3D}	ESA TW fit factor (hypervelocity regime)
$\cos\theta^n$	Cosine term exponent (ballistic and hypervelocity regimes)

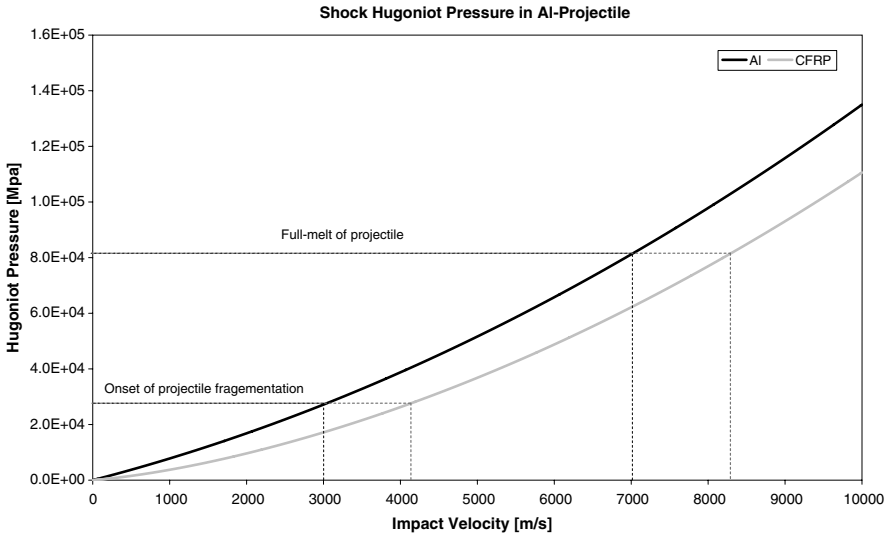

Fig. 5. Shock-Hugoniot curves for Al-projectile impact on Al and CFRP targets. Al projectile and Al target properties used in calculation: $\rho_p = 2.7$ g/cm^2, $c_B = 5300$ m/s, $K = 0.94$; CFRP target properties: $\rho_{ob} = 1.55$ g/cm^2, $c_B = 1763$ m/s, $K = 1.93$.

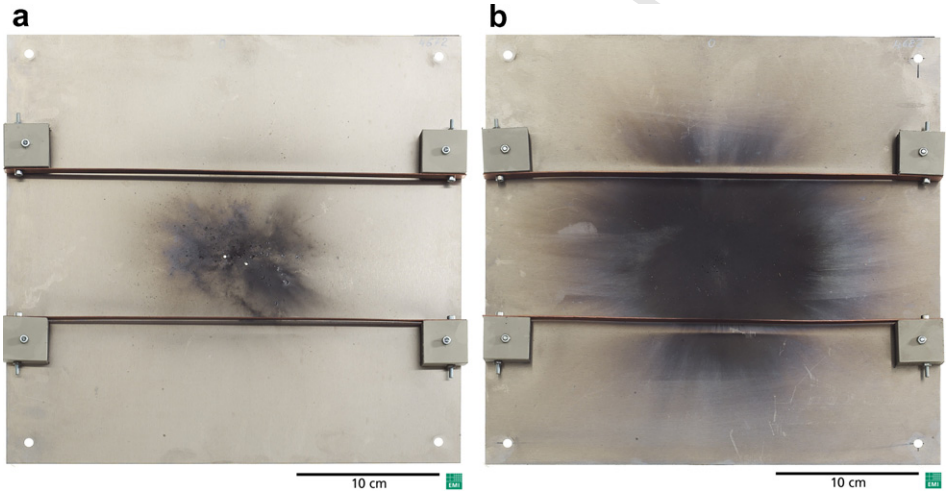

Fig. 6. Witness plate damage. (a) EMI No. S-4672, normal impact (0°) of a 4.0 mm projectile at 3.57 km/s; (b) EMI No. S-4682, normal impact (0°) of a 4.0 mm projectile at 7.75 km/s.

In addition to these parameters, additional terms are available for modification to fit the curve to any future experimental data. These terms are:

- Exponent and coefficient of the t_w term in the equation describing the BL in the ballistic regime.
- Exponent and coefficient of the t_w term in the equation describing the BL in the hypervelocity regime.
- Exponent and coefficient of the S_2 term in the equation describing the BL in the hypervelocity regime.

Due to a lack of variation of the witness plate thickness and witness plate standoff in the experiments, the coefficients and exponents used in the ESA Triple Wall equations were adopted here (with one exception: the exponent of the t_w-term in the BLE equation for the low velocity regime). Obviously, these coefficients can be adjusted pending the availability of corresponding impact test data.

(7) The impact velocities corresponding to the transition between ballistic- and shatter impact velocity regimes (v_1) as well as the shatter- and hypervelocity impact regimes (v_2) represent impact-induced Hugoniot pressures that cause the onset of fragmentation and full melt of the impactor, respectively. For Al–Al impact, limit velocities of 3 and 7 km/s are commonly used (see e.g. Christiansen, 1993). The material properties that affect the Hugoniot pressures generated in the projectile and target during hypervelocity impact are related to the material densities, bulk sound speeds, and particle velocity–shock velocity relationships. A 1D shock-Hugoniot analysis was performed to determine approximate transition velocities for Al-CFRP impact. The results of the analysis are shown in Fig. 5. The shock velocity–particle velocity relationships for Al and CFRP were taken from Schaefer

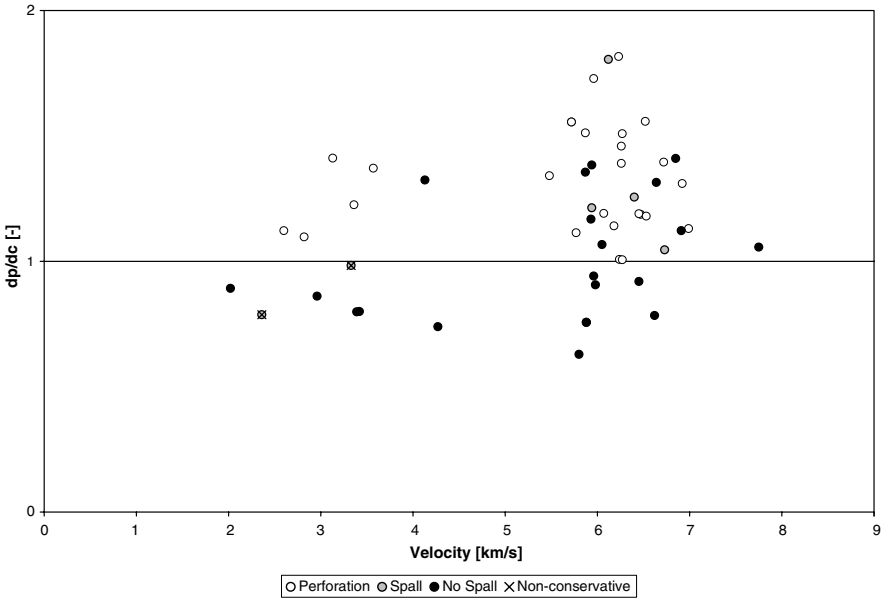

Fig. 7. Comparison of predicted and actual experimental results.

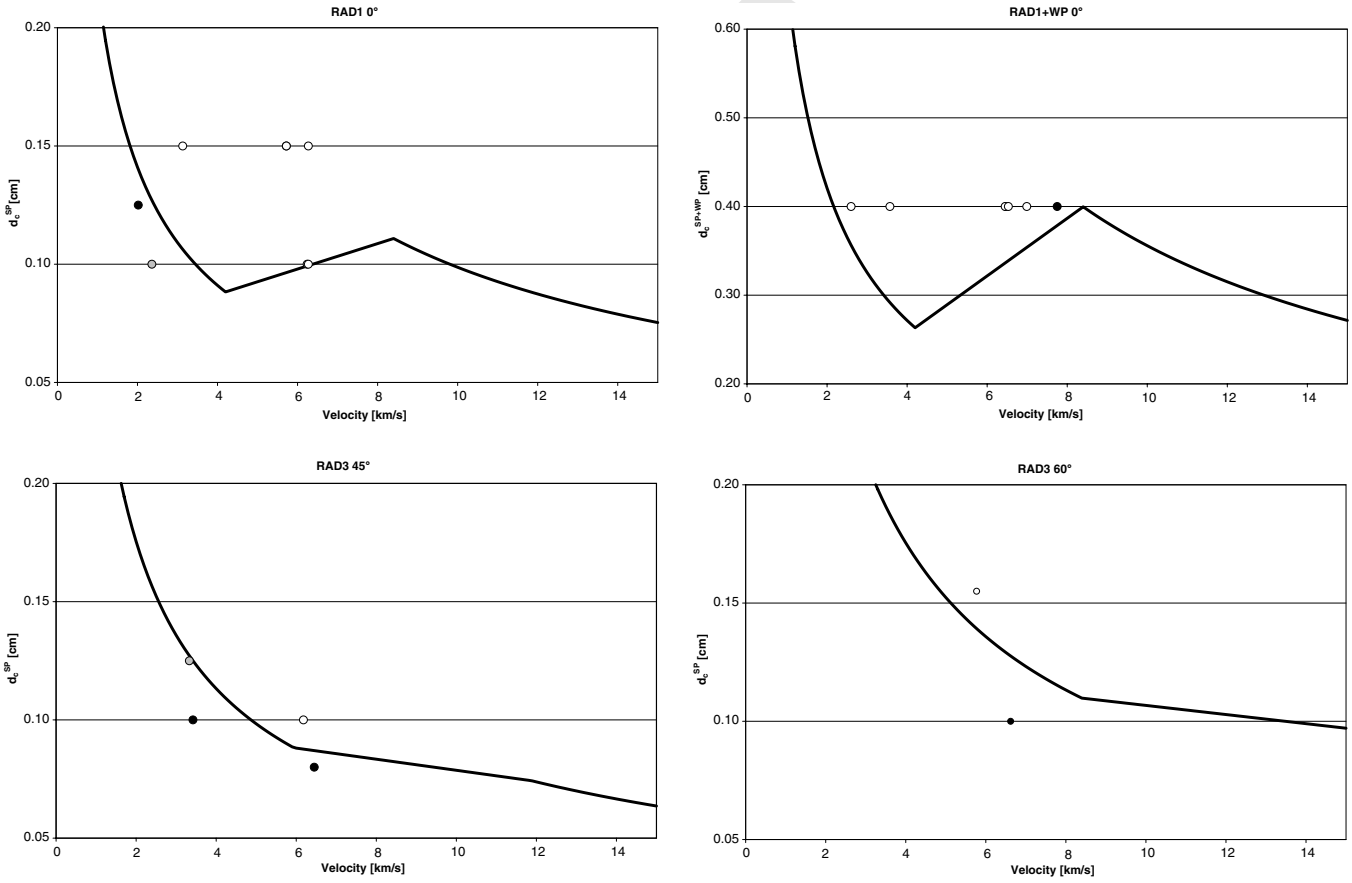

Fig. 8. Predicted BLCs and experimental results. Upper left: RAD1 at 0°; Upper right: RAD1+WP at 0°; Lower left: RAD3 at 45°; Lower right: RAD3 at 60°.

(2001) and Machens (2004), respectively. More details of the shock-Hugoniot analysis are given in Schaefer and Ryan (2005).

In Fig. 5, it is obvious that impact of Al on CFRP generates lower Hugoniot pressures in the Al-projectile compared to impact on an Al target at a constant impact

Table 7
Assessment of the BLE predictions for each structure versus experimental results

Structure	Angle (°)	Assessment of results	Comments
RAD1	0	−	One (from 8) NC prediction
	45	+	One (from 5) VC prediction
	60	?	Results only for >BL
RAD1 + WP	0	++	
	45	0	Results only for <BL
RAD2	0	+	One (from 3) SC prediction
	45	++	
RAD3	0	++	One (from 8) SC prediction
	45	−	One (from 4) NC prediction
	60	++	
RAD3 + WP	0	?	Results only for >BL
GOCE	0	++	
	45	?	Results only for <BL
GOCE + WP	0	+	One (from 2) VC prediction
SAX	0	0	One (from 2) VC prediction
SAX + WP	0	?	Results only for >BL
	45	0	One result, VC prediction
H/P	0	?	Results only for >BL

++, good – result predicted correctly;
+, slightly conservative – experiment result NSP, prediction P, d_p:$d_c \leqslant 1.2$;
0, very conservative – experiment result NSP, prediction P, d_p:$d_c > 1.2$;
−, non-conservative – experiment result P, prediction NSP;
?, inconclusive – experimental results do not allow assessment of equation accuracy.

Table 8
Structural configurations from literature used for further assessment of the SRL BLE accuracy

Mission	Reference	CFRP facesheets				Honeycomb	
		t (mm)	Material	Density (g/cm)	Stacking	Configuration	t (mm)
Envisat	Schaefer	1.1	M40/NCHM 914 fabric	1.579	$(3\times(0/\pm 60))$	3/16-.0015-5056P	45
Unknown	Taylor	1.62	HMF371/7714B fabric	1.825	$(0/90)_S$	5.2 1/4-.0025-3003	45
AXAF (A)[b]	Frost	0.254	M60J/954-2A u.d. ply	1.66[a]	Unknown	Unknown	15.875
AXAF (B1)[c]	Frost	0.762	M60J/954-2A u.d. ply	1.66[a]	Unknown	Unknown	15.875
AXAF (B2)[c]	Frost	0.762	P100/unknown u.d. ply	1.66[a]	Unknown	Unknown	15.875
AXAF (C)[b]	Frost	0.508	M60J/954 u.d. ply	1.66[a]	Unknown	Unknown	6.35
AXAF (D)[b]	Frost	1.016	M60J/954 u.d. ply	1.66[a]	Unknown	Unknown	6.35
AXAF (E)[b]	Frost	1.524	M60J/954 u.d. ply	1.66[a]	Unknown	Unknown	6.35
AXAF (F)[d]	Frost	0.406	M60J/954-3 u.d. ply	1.66[a]	Unknown	Unknown	6.35

[a] Calculated from density of constituents assuming fibre volume content of 60%.
[b] MLI attached to outer side of front facesheet, see MLI type ABC in Frost and Rodriguez (1997). Estimated AD = 791 g/m^2.
[c] MLI attached to outer side of front facesheet, see MLI type ST in Frost and Rodriguez (1997). Estimated AD = 791 g/m^2.
[d] MLI attached to outer side of front facesheet, see MLI type KF in Frost and Rodriguez (1997). Estimated AD = 516 g/m^2.

velocity. The Hugoniot pressures determined in the 1D shock analysis at which the onset of fragmentation and full melt of the projectile occur (i.e. 3 and 7 km/s, respectively for Al-on-Al impact) were reproduced by impact on CFRP at velocities of 4.2 and 8.4 km/s, respectively. Thus, the transition velocities for the ballistic limit equation were set as:

Transition ballistic–shatter regime: 4.2 km/s.

Transition shatter–hypervelocity regime: 8.4 km/s.

The transition velocities are derived for ballistic limit prediction of the stand-alone CFRP/Al HC SP. When considering penetration of the thin Al-plate located behind the CFRP/Al HC SP, the projectile is shocked twice (sandwich panel front and rear facesheets) and therefore the fragmentation performance is expected to improve, i.e. higher fragmentation and melting at lower impact velocities (similar to the multi-shock shielding concept (Cour-Palais and Crews, 1990)). Fig. 6 shows the Aluminium witness plate for impacts on the RAD1 panel.

For impact at 3.57 km/s, it appears from the witness plate damage that fragmentation of the projectile has occurred and therefore a ballistic–shatter regime transition velocity of 4.2 km/s (as used for the sandwich panel) is too high. Fragment damage is also seen on the witness plate used in Exp. 4671 ($v = 2.6$ km/s). For impact at 7.75 km/s, there are still craters visible in the witness plate which are caused by the impact of individual Aluminium fragments. The derivation of an analytical solution to

Table 9
Assessment of the BLE predictions versus experimental results for literature data sets

Structure	Angle (°)	Assessment of results				Comments
ENV	0		+			One (from 3) VC prediction
ENV+MLI	0			0		One (from 2) VC prediction
Taylor	0	++				
	15		+			One (from 2) SC prediction
	45		+			One (from 3) SC prediction
	60				?	No results >BL
	75				?	No results >BL
AXAF-A	0			0		One (from 3) VC prediction
AXAF-B1	0				?	No results <BL
AXAF-B2	0			0		One (from 2) VC prediction
AXAF-C	0			0		One (from 3) VC prediction
AXAF-D	0			0		One (from 4) VC prediction
AXAF-E	0		+			One (from 4) SC prediction
AXAF-F	0			0		One (from 2) VC prediction

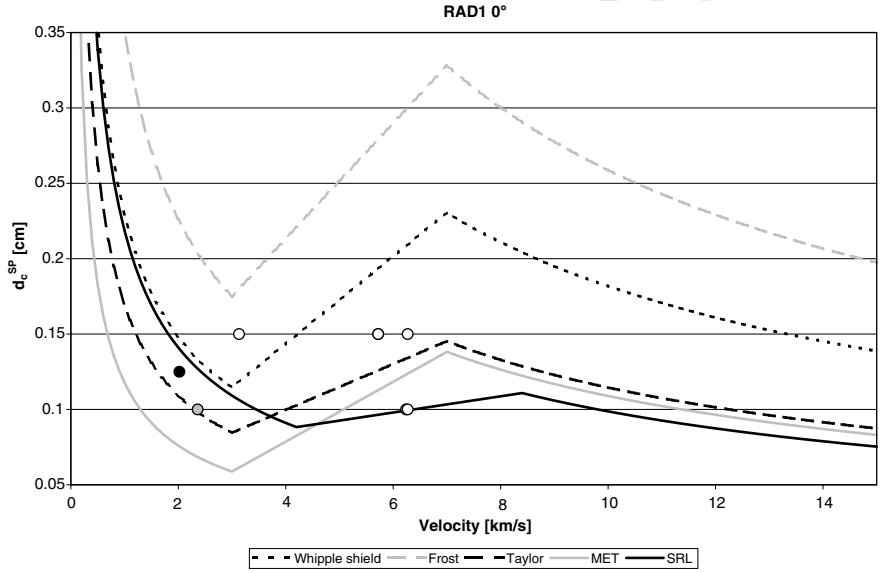

Fig. 9. RAD1 CFRP/Al HC SP; experimental data and calculated BLCs for 0° impact using predictions from Christiansen, Frost, Taylor, MET and Eqs. (4)–(6).

determine the increase in internal pressure at each shock interface was not possible. Additionally, as all impact tests performed to assess the ballistic limit of the thin Al-plate show impact of solid projectile fragments (i.e. all within shatter regime), the transition limits cannot be bounded. As such, the transition velocities determined for the CFRP SP are used for prediction of the thin Al-plate located behind the SP.

All other assumptions and coefficients were adopted from the ESA Triple Wall equation.

3.3. Application of the SRL BLE for CFRP/Al HC satellite structures

The quality of the equation can be assessed by evaluating the predictive performance across the entire range of structures and impact conditions investigated. In Fig. 7, the experimental results of Tables 2 and 3 are plotted in terms of the projectile diameter (d_p) to predicted critical diameter (d_c) ratio. In this figure, results above unity represent predicted failure and results less than one represent a "no detached spall" prediction.

For 44 out of 55 experiments, covering 10 different structures, three different impact angles and an impact velocity range of 2.02–7.75 km/s the equation correctly predicted the result. This represents a success rate of 80%.

In Fig. 8 the calculated ballistic limit curves (BLCs) are plotted for a selection of structures tested during the experimental campaign, which includes both stand-alone sandwich panels and those including witness plates. The impact experiment results are also shown in the figures.

An overview of the predictive accuracy of the SRL equation, organised by structure, is given in Table 7. Of the 55 experiments, 40 (73%) showed a "good" prediction, 5

experiments (9%) were predicted slightly conservatively, 8 experiments (15%) were predicted very conservatively, and 2 experiments (4%) were non-conservatively predicted.

3.4. Application of the SRL BLE to additional CFRP/Al HC satellite structures

Prior to this study, the amount of hypervelocity impact test data available in the literature for composite sandwich panels was limited. Impact data related to witness plate, or other types of secondary damages induced by HVI on composite structure walls was almost non-existent. A comprehensive literature survey has been used to further assess the SRL equation predictive accuracy of the SRL equation. Experimental results of Lambert et al. (2001), Taylor et al. (1999) and Frost and Rodriguez (1997) are given in Table 9.

A short description of the structures tested in these studies is given in Table 8.

For 28 out of 37 experiments, covering 10 different structures, five different impact angles and an impact velocity range of 4.80–7.26 km/s the equation correctly predicted the result. This represents a success rate of 75.7%. Additionally, 3 experiments (8%) were predicted slightly conservatively, and 6 experiments (16%) were predicted very conservatively. No predictions were non-conservative.

The predictive accuracy, organised by structure, is given in Table 9.

4. Comparison with current BLEs for CFRP/Al HC sandwich panels

Schaefer et al. (2004) identified four different approaches for predicting the ballistic limit of CFRP/Al HC sandwich panel structures (the Whipple shield, Taylor, Frost, and MET approaches as defined previously). Predictions of the impact test experimental results calculated using these approaches was compared to assess the improvement in the BL prediction capability of the new equation.

In Figs. 9 and 10, BLCs of a selection of the structures described in Tables 1 and 8 are shown, along with any experimental data, calculated using the various approaches introduced previously. These figures were used to assess the accuracy of these existing techniques, and the improvement of the BL prediction capability afforded by the new equation.

Predictions of all experimental impact tests presented in Table 4, as well as that from Schaefer (1996), Taylor (1999) and Frost (1997) were calculated using the Whipple shield. Frost, Taylor and MET approaches. A comparison of the results with the predictions made using Eqs. (4)–(6) is given in Fig. 11.

In Fig. 11, it can be noted that for the test campaign and literature data analysed:

The Whipple-shield approach is non-conservative (50% of all perforating impact experiments were non-conservatively predicted). This characteristic is not structure or parameter specific, i.e. non-conservative predictions are made across the range of structures and parameters (e.g. thin honeycomb, thick facesheet, etc.). The best performance of this equation is with application on thin-honeycomb structures (RAD3, AXAF) at normal impact.

The Frost approach is non-conservative (75% of all perforating impact experiments were non-conservatively predicted). This characteristic is not structure or parameter specific, i.e. non-conservative predictions are made across the range of structures and parameters (e.g. thin honeycomb, thick facesheet, etc.). The best performance of this equation is with application on thin-honeycomb structures with MLI attached (AXAF) at normal impact.

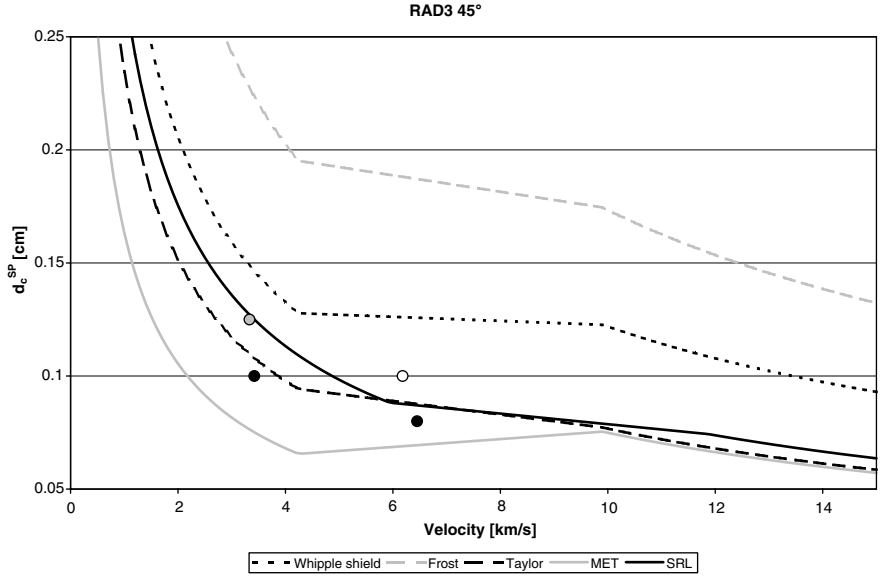

Fig. 10. RAD3 CFRP/Al HC SP; experimental data and calculated BLCs for 45° impact using predictions from Christiansen, Frost, Taylor, MET and Eqs. (4)–(6).

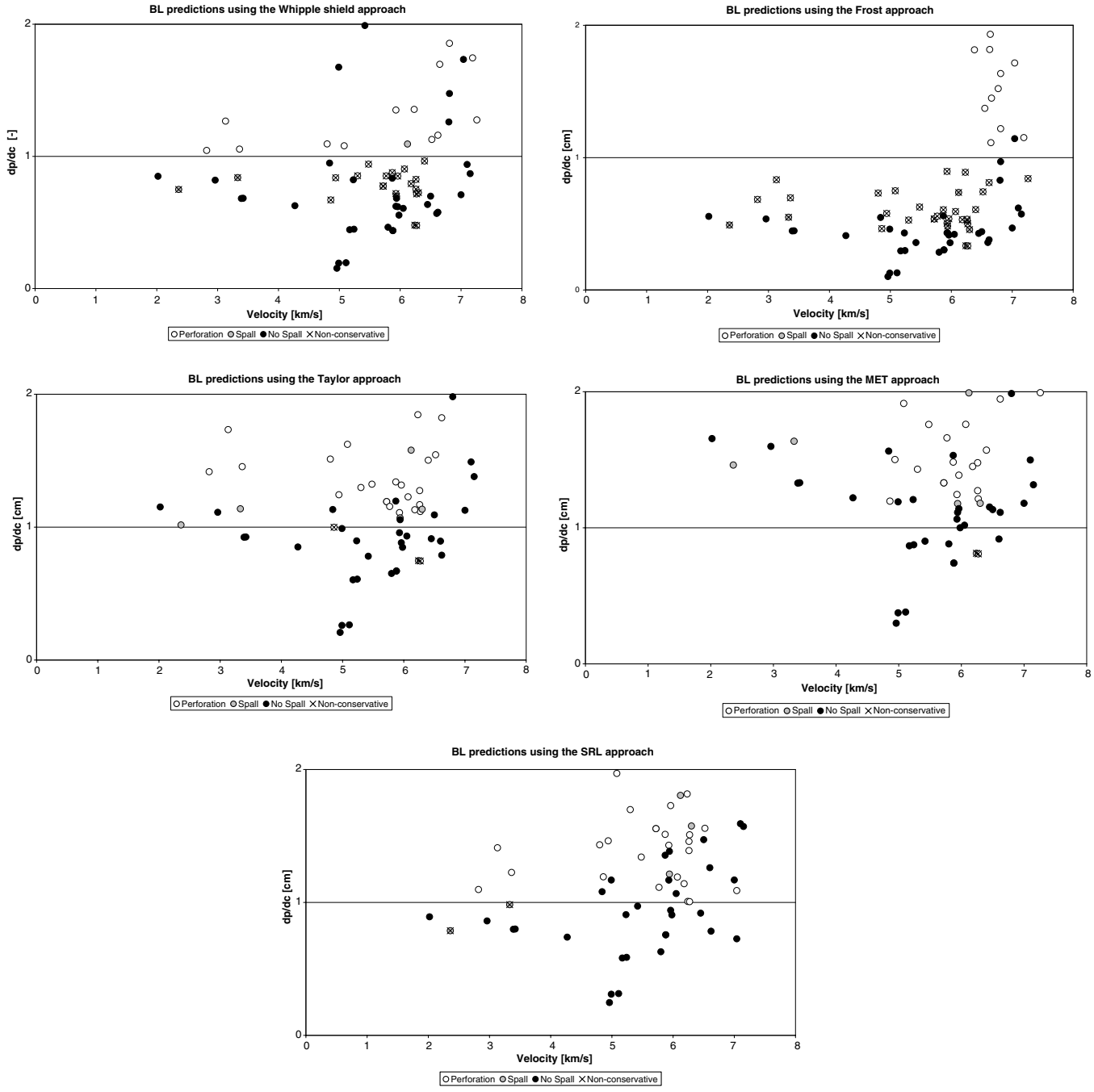

Fig. 11. Comparing the accuracy of the various BLEs for all sandwich panel experimental data; upper left: Christensen approach; upper right: Frost approach; middle left: Taylor approach; middle right: MET approach; lower: new approach presented in this paper.

The Taylor approach shows good agreement with the experimental results (81% of impact test results predicted correctly). Of the 44 perforation/spall impact experiments, only 3 predictions (6.8%) are non-conservative.

The MET approach shows good agreement with the experimental results (68% of impact test results predicted correctly). Of the 44 perforation/detached spall impact experiments, only 2 predictions (4.5%) are non-conservative.

The new approach gives good agreement with the experimental results (81% of impact test results predicted correctly). Of the 44 perforation/detached spall impact experiments, only 2 predictions (4.5%) are non-conservative (both detached spall).

5. Summary and conclusions

In this paper, a new ballistic limit equation for CFRP/Al HC satellite structure walls has been presented. This equation is applicable for ballistic limit prediction of stand-alone sandwich panels, and for thin Al plates located at a standoff behind these sandwich panels. The thin Al-plates are representative of internal systems, e.g. lid of an

Please cite this article in press as: Ryan, S. et al., A ballistic limit equation for hypervelocity impacts ..., J. Adv. Space Res. (2007), doi:10.1016/j.asr.2007.02.032

electronic box, metallic vessel, etc. Ballistic limit impact tests have been performed on six representative CFRP/Al HC sandwich panels, and the results of these impact tests have been used to empirically adjust the new equation. In addition, three additional sets of impact test data from literature were considered in order to provide a more thorough assessment of the equation's performance.

A one-dimensional Hugoniot-shock analysis was performed to review the limit velocities representing transition from the ballistic to the shatter regime (onset of projectile fragmentation) and from the shatter to the hypervelocity regime (full melt of projectile). From this preliminary analysis, transition velocities of 4.2 and 8.4 km/s were defined for impact of Al on CFRP. Clearly, this technique provides only an approximate indication of fragmentation velocities, and it is therefore suggested that additional investigation is required.

The new equation was shown to provide good agreement with the impact experiment results, for both the stand-alone sandwich panels and those including thin Al plates at a standoff. For sandwich panels with thin honeycomb cores and MLI attached to the front CFRP facesheet (e.g. AXAF) the predictions tended towards being "very conservative". This is possibly due to an oversimplification of the effect of high surface-weight MLI (e.g. MLI incorporating betacloth, silver Teflon, etc.) on a projectile impacting at hypervelocity. Further characterisation of the effect of MLI in hypervelocity impact tests is required. An alternative cause may be statistical weighting of the SRL equation. Given that the fit factors are empirically adjusted based on available experimental data, the equation will be biased towards configurations for which more experimental data is available. As the H/P panel was the only structure used in adjusting the fit parameters of the SRL equation which has a comparatively thin facesheet with the AXAF panel, and for this structure only one test data point was available, any statistical weighting inherent in the SRL equation will be subsequently exposed.

Four existing approaches for ballistic limit prediction of CFRP/Al HC sandwich panels were additionally reviewed in this paper using the new impact test data. It was found that the approach of Frost and Rodriguez (1997) and that based on the Christiansen/Cour-Palais Whipple-shield equation (Christiansen, 1993) were non-conservative across the range of configurations considered, while the approach of Taylor et al. (1999) and Schaefer et al. (2004) approach provided good agreement, though were slightly conservative. The approach introduced in this paper gave comparable or superior results over the four existing approaches discussed in predicting the BL of stand-alone sandwich panels, while additionally providing the means of determining mechanical damage to thin Al plates located behind the structure wall.

Acknowledgement

This study was performed in the framework of ESA Contract 16721/02/NL/CK "Composite Materials Impact Damage Analysis".

References

Christiansen, E. Design and performance equations for advanced meteoroid and debris shields. International Journal of Impact Engineering 14, 145–156, 1993.

Cour-Palais, B., Crews, J. A multi-shock concept for spacecraft shielding. International Journal of Impact Engineering 10, 135–146, 1990.

Drolshagen, G., Borge, J. Meteoroid/Debris Impact Analysis (ESABASE/DEBRIS:) Technical Description. ESA-ESTEC, Noordwijk, Germany, Report No. ESABASE-GD-01/1, 1992.

Frost, C., Rodriguez, P. AXAF hypervelocity impact test results, in: Proceedings of the 2nd European Conference on Space Debris, ESA-ESOC, Darmstadt, Germany, 17–19. March, ESA SP-393, 1997.

Jex, D., Miller, A., MacKay, C. The characteristics of penetration for a double-sheet structure with honeycomb. NASA Marshall Space Flight Center, Alabama, USA, NASA TM X-53974, 1970.

Lambert, M., Schaefer, F., Schneider, E. Impact damage on sandwich panels and multi-layer insulation. International Journal of Impact Engineering 26, 369–380, 2001.

Machens, M. Shock properties of a carbon fibre composite for space applications. FhG-EMI, Freiburg, Germany, EMI Report No. I-36/04, 2004.

Schaefer, F. Hypervelocity impact testing. impacts on pressure vessels. Final Report to ESA Contract No. 10556/93/NL/PP(SC), FhG-EMI, Freiburg, Germany, EMI Report No. I-27/01, 2001.

Schaefer, F., Destefanis, R., Ryan, S., Riedel, W., Lambert, M. Hypervelocity impact testing of CFRP/Al Honeycomb satellite structures, in: Proceedings of the 4th European Conference on Space Debris, ESA-ESOC, Darmstadt, Germany, 18–20 April, ESA SP-587, 2005.

Schaefer, F., Ryan, S. Composite materials impact damage analysis. Final Report to ESA Contract No. 16721/02/NL/CK, FhG-EMI, Freiburg, Germany, EMI Report No. I-69/05, 2005.

Schaefer, F., Schneider, E., Lambert, M. Review of ballistic limit equations for CFRP structure walls of satellites, in: Proceedings of the 5th International Symposium on Environmental Testing for Space Programmes, ESA-ESTEC, Noordwijk, Netherlands, 15–17 June, ESA SP-558, 2004.

Schneider, E., Schaefer, F. Hypervelocity impact research – acceleration technology and applications. Advances in Space Research 28 (9), 1417–1424, 2001.

Taylor, E., Herbert, M., Vaughan, B., McDonnell, J. Hypervelocity Impact on Carbon Fibre Reinforced Plastic/Aluminium honeycomb: comparison with Whipple bumper shields. International Journal of Impact Engineering 23, 883–893, 1999.

Taylor, E. Computational study of hypervelocity impact onto Whipple bumpers and sandwich plates with honeycomb core, ESA/ESTEC, Noordwijk, Netherlands, Report No. EWP-2029, 1999.